

Quantum dissection of a covalent bond

Norm M. Tubman¹ and D. ChangMo Yang¹

¹*University of Illinois at Urbana-Champaign, Urbana, Illinois, USA*

We propose that spatial density matrices, which are singularly important in the study of quantum entanglement¹, encode the electronic fluctuations and correlations responsible for covalent bonding. From these density matrices, we develop tools that allow us to analyse how many body wave functions can be broken up into real space pieces. We apply these tools to the first row dimers, and in particular, we address the conflicting evidence in the literature about the presence of an inverted fourth bond and anti-ferromagnetic correlations in the C₂ molecule²⁻⁵. Our results show that many body effects enhance anti-ferromagnetic fluctuations but are not related to the formation of an inverted fourth bond. We identify two inverted bonds in the C₂ molecule and establish their correspondence to the bonds in the Be₂ molecule. Additionally, we provide a new interpretation of the Mayer index⁶, introduce partial bonds to fix deficiencies in molecular orbital theory, and prove the Hartree-Fock wave function for C₂ is not a triple bond. Our results suggest that entanglement-based methods can lead to a more realistic treatment of molecular and extended systems than possible before.

Comparing the results from different theories of bonding is difficult, as these theories often access very different properties with widely varying constraints on the wave function. Common types of bonding analysis include the use of molecular orbital (MO) theory to calculate bonding/anti-bonding pairs⁷, density-matrix renormalization group (DMRG) to calculate mutual information of molecular

orbitals⁸, and valence bond (VB) theory to find the dominant spin configurations^{2,5}. These tools are complemented by several different bond indices^{6,9}, and theories based on single-particle properties, such as Bader analysis¹⁰.

Arguably, the real space degrees of freedom of a many body wave function are the main quantities of interest that bonding analysis techniques are trying to access. VB theory comes close in this regard, as the optimised orbitals are partially localised. However, this localisation requires a highly constrained wave function (see Table 2 for C_2 energies). Other techniques attempt to capture various properties related to bonding, but there has been a lack of consensus of which provide the best description. For instance, new theoretical studies of the C_2 dimer have challenged conventional descriptions of covalent bonding. As an example of the divergent views on the C_2 molecule²⁻⁵, a recent VB study suggested an inverted fourth bond caused by many body correlations², while a follow-up study showed the molecule is anti-ferromagnetically coupled⁵. Recent DMRG simulations do not have access to the proper degrees of freedom to settle the issue¹¹, and it is not clear that other techniques can be used to probe such features. Another problem in describing covalent bonds is that many of these theories can only be applied to very specific wave functions. Explicit many body theories such as mutual information studies in DMRG and spin configuration identification in VB theory, cannot be applied to general wave functions optimized with variational Monte Carlo (VMC) or Hartree-Fock (HF) wave functions. This makes analysing even HF wave functions challenging. Although there are many systems for which MO theory provides a useful description of bonding properties, the C_2 molecule is not one of them.

Real space density matrices can be used as a general tool to analyse bonds. Their usefulness in determining quantum entanglement properties has garnered widespread recognition in the past decade^{1,12–15}, and the idea itself goes back even further^{16,17}. These density matrices have been instrumental in recent breakthroughs with regards to applications in string theory¹⁸, black holes¹, and topological phase transitions¹⁹. These same density matrices also happen to encode how molecules form covalent bonds. This analysis involves dividing a quantum system into two spatial regions, A and B, which can be an arbitrary geometric bi-partition of space. The degrees of freedom in region B are integrated out, leaving a density matrix that only exists in region A. This is written as $\hat{\rho}_A = \text{Tr}_B\{\hat{\rho}_{AB}\}$, where Tr_B is a trace over the degrees of freedom in region B and $\hat{\rho}_{AB}$ is the full density matrix of a system. The density matrix $\hat{\rho}_B$ can likewise be defined with a trace over region A. For the diatomic molecules in this work, we will take regions A and B to be the half spaces on either side of the perpendicular bisector of the molecular axis.

A Schmidt decomposition of a wave function^{17,20} can be used to relate the spatial density matrices to the full many-body wave function as

$$|\Psi\rangle = \sum_i s_i |A_i\rangle |B_i\rangle . \quad (1)$$

Here, $|A_i\rangle$ and $|B_i\rangle$ are eigenvectors of $\hat{\rho}_A$ and $\hat{\rho}_B$ respectively, and $|s_i|^2$ are the eigenvalues. The eigenvalues of $\hat{\rho}_A$ and $\hat{\rho}_B$ are in one-to-one correspondence and are equal, regardless of the partition of space. For the symmetric half-space partition of a homonuclear dimer, these density matrices have mirror-symmetric eigenvectors.

For a single-determinant wave function, Eq. 1 reduces to a more compact form

$$|\Psi\rangle = \prod_{i=1}^N \left(\sqrt{\lambda_i} c_{i,A}^\dagger + \sqrt{1 - \lambda_i} c_{i,B}^\dagger \right) |0\rangle \quad (2)$$

with 2^N terms, where N is the number of electrons²⁰. In this equation, the values of λ are in the range $0 \leq \lambda \leq 1$ and determine the probability distribution of electrons between regions A and B. The operator $c_{i,A}^\dagger$ creates a single-particle orbital that has support only in region A, and $c_{i,B}^\dagger$ creates a single-particle orbital that has support only in region B. Quite simply, this equation says that an electron i is found with probability λ_i in region A and probability $1 - \lambda_i$ in region B. The case $\lambda = 1$ corresponds to an electron that is completely localised in region A and $\lambda = 0$ corresponds to an electron completely localised in region B. The case of $\lambda = 1/2$ corresponds to an electron with equal probability to be in either regions A and B. Examples of region A orbitals are plotted for C_2 in Fig. 3.

By introducing a single-determinant wave function in the form of Eq. 2, we have provided a new theory for analysing covalent bonds. We study its properties by first demonstrating its relationship with MO theory. In MO theory, the occupation of a bonding orbital by two electrons is implicitly interpreted as them being equally shared by the two atoms. In Eq. 2, this corresponds to two electrons with $\lambda = 1/2$ which can be expanded as

$$|\Psi\rangle = \frac{1}{2} |\phi_{\uparrow 1,A} \phi_{\downarrow 1,A}\rangle + \frac{1}{2} |\phi_{\uparrow 1,B} \phi_{\downarrow 1,A}\rangle + \frac{1}{2} |\phi_{\uparrow 1,A} \phi_{\downarrow 1,B}\rangle + \frac{1}{2} |\phi_{\uparrow 1,B} \phi_{\downarrow 1,B}\rangle . \quad (3)$$

These four terms have a simple interpretation: 25% chance both electrons are localised in region A, 25% chance a spin-up electron is localised in region A, 25% chance a spin-down electron is localised in region A, and 25% chance that neither are localised in region A.

When four electrons occupy a pair of bonding and anti-bonding orbitals, they are interpreted as not contributing to the bonding in MO theory. The corresponding picture given by Eq. 2 is a group of four λ values $(0, 0, 1, 1)$, representing two electrons in region A and two electrons in region B. For this case, Eq. 2 reduces to a single term. Although λ can take values from a continuous range, MO theory only attempts to describe $\lambda = 0, 1/2$, or 1. For the molecules considered in this work, the ground state wave functions are mirror-symmetric with respect to the half space. This leads to an important constraint on the values of λ . Whenever a spin-up electron is partially localised in region A, another spin-up electron must be localised in region B to maintain mirror symmetry of the charge between regions A and B. To maintain spin symmetry, two more spin-down electrons must be introduced. This couples electrons into groups of four such that $\lambda_{1,2,3,4} = (\lambda, \lambda, 1 - \lambda, 1 - \lambda)$. The orbitals for the first two electrons are the same except they have opposite spin quantum numbers, and the orbitals for the third and fourth electrons are also the same but with opposite spin. For these symmetric diatomic molecules, all electrons must come in groups of four, with only one exception, $\lambda = 1/2$. In this case, it is possible to maintain the proper space and spin symmetry with only two electrons. This is because mirror-symmetric orbitals can occur only for $\lambda = 1/2$.

The values of λ for HF wave functions are listed in Table 1. We see that the perfectly localised groups of four $(0, 0, 1, 1)$ and delocalised groups of two $(1/2, 1/2)$ are the only grouping of electrons needed to describe most of the molecules. However, in the case of C_2 and Be_2 , there are groupings of four electrons that are not perfectly localised and are not described by MO theory. For C_2 , there has always been some uncertainty with in how to describe the valence electrons. Various

bond indices⁶ yield values between 3 and 4, which suggests the possibility of three strong bonds and one weak bond². This is shown not to be the case in Table 1, where four of the electrons have 50% probability of being on either atom (corresponding to orbitals with π -like symmetry, as shown in Fig. 3), while each of the remaining four electrons correspond to 81% partial localisation. An interesting aspect of this localisation is that the orbital amplitudes for the paired orbitals $\lambda = 0.81$ and $\lambda = 0.19$ are not symmetric. These orbitals are shown in Fig. 3 and have similar properties as what has been previously interpreted as an inverted bond. For $\lambda = 0.81$, the half-space orbital has rotational symmetry around the bonding axis, and the corresponding orbital with $\lambda = 0.19$ also has this symmetry but changes sign along the bonding axis and has charge accumulation away from the bond. A key difference from our result and the previously described inverted bond², is that we predict two of them from the HF wave function. Our results definitively show that a multi-determinant wave function is not necessary to capture the inverted bond — it has always been present in the HF wave function.

The result from our symmetry analysis explicitly prevents the HF wave function of the C_2 molecule from being a triple bond. For a triple bond to occur in C_2 , six of the valence electrons must be grouped differently from the remaining two localised valence electrons. But symmetries force localised electrons to come in groups of four. There are only three possible groupings for eight electrons: a quadruple bond $(\frac{1}{2}, \frac{1}{2}), (\frac{1}{2}, \frac{1}{2}), (\frac{1}{2}, \frac{1}{2}), (\frac{1}{2}, \frac{1}{2})$; a double bond with two partial bonds $(\frac{1}{2}, \frac{1}{2}), (\frac{1}{2}, \frac{1}{2}), (\lambda, \lambda, 1 - \lambda, 1 - \lambda), (\lambda', \lambda', 1 - \lambda', 1 - \lambda')$; four partial bonds $(\lambda, \lambda, 1 - \lambda, 1 - \lambda), (\lambda', \lambda', 1 - \lambda', 1 - \lambda')$. Therefore it is impossible for eight valence electrons to form a triple bond in HF theory without breaking spin and space symmetries.

The set of values for λ provide a complete description of the bonding fluctuations in HF theory, as the full HF wave function can be written in terms of these modes as shown in Eq. 2. We have discussed MO theory as an incomplete theory of electron fluctuations, which can be fixed by incorporating the idea of partial localisation. To add this idea into standard MO theory, we suggest simple modifications to hybridisation diagrams. The standard hybridisation from MO theory is shown in Fig. 1a, and our modified diagram is shown in Fig. 1b. Orbitals that correspond to the standard 0, 1/2, and 1 are unchanged, as those are already included in MO theory. For non-standard λ values, we indicate the two orbitals, which form the grouping, by a dashed line, and we include the λ value near one of the MOs. This analysis also suggests a correspondence between the Mayer index and Eq. 2, as this index also has an interpretation based on the second moment of the particle fluctuations in the case of HF wave functions²¹. From Eq. 2 we see the entire power spectrum of fluctuations, including the second moment, can be calculated from the λ values.

To analyse correlated wave functions, we begin by introducing model state entanglement spectra in which to compare our numerical spectra²². The entanglement spectra are defined as the eigenvalues of $\hat{\rho}_A$, and generally they are broken up into block-diagonal sectors, which for molecules will consist of the number of electrons in region A and the spin polarisation (N_A, S_z). In our entanglement theory, perfect bonds of bond order ν are given by setting $\lambda = 1/2$ for every mode as

$$|\Psi^{(\nu)}\rangle = \prod_{\sigma} \prod_{i=1}^{\nu} (\sqrt{1/2}c_{\sigma i,A}^{\dagger} + \sqrt{1/2}c_{\sigma i,B}^{\dagger}) |0\rangle . \quad (4)$$

The core electrons and filled bonding/anti-bonding modes are described by $\lambda = (0, 0, 1, 1)$, and can be included into the above wave function forms without changing the coefficients in front of

the terms. The defining characteristic of these entanglement spectra is the number of eigenvalues in each block-diagonal sector and a single number, which is the magnitude of these eigenvalues. This is plotted for single, double, and triple bonds in Fig. 1c.

In Fig. 2 we present the entanglement spectra of four different molecules from two types of wave functions: the HF wave function and a wave function optimised with VMC^{23,24}. spectra are plotted in Fig. 2. A summary of different wave functions and their energies for C_2 is given in Table 2. We see the HF spectrum, which can be derived from Table 1 and Eq. 2, has the same form as a perfect single bond in the case of Li_2 and a perfect triple bond in the case of N_2 . This picture remains essentially unchanged for the many-body wave functions. The effect of Coulomb repulsion reduces the probability of sectors with large charge fluctuations. One distinct feature present is a gap in the spectrum. The number of modes in each sector below the gap corresponds to that of our model spectra. This is similar to what is seen in the fractional quantum Hall wave functions²², in which the entanglement spectrum below the gap is called the *universal* part of the spectrum and one can count the modes in the various sectors to determine what type of fractional quantum Hall system is present. The modes below the gap have the highest probability and capture the essential physics of the bond. This also makes this analysis useful for more complicated molecules, which are not symmetric, as the number of eigenvalues below the gap will remain unchanged with regards to asymmetries. Using the counting of the eigenmodes below the gap, we can identify N_2 as a triple bond and Li_2 as a single bond, even for the VMC-optimised wave functions. Such simplicity is not evident for C_2 .

There are many interesting properties of the C_2 molecule that can be determined from the entanglement spectrum. To address recent VB studies, we are concerned specifically with the possibilities of anti-ferromagnetic correlations^{5,11}, which are described as an increase in probability of electrons of like spin accumulating on the first atom, and likewise for the second atom but with the opposite spin. These anti-ferromagnetic correlations can be identified with the quantum numbers of the block diagonal sectors in $\hat{\rho}_A$ and we can quantitatively compare the difference between HF, full valence CAS, and the VMC-optimised wave functions. From Fig. 2 and Table 3 we see that there is a significant increase in anti-ferromagnetic correlations, and in particular the probability of the dominant eigenvalues in the sectors $N_A = 6, S_z = \pm 4$ increase by an order of magnitude over the same eigenvalues in the HF wave function. The sectors $N_A = 5, S_z = \pm 3$ are also enhanced, though less significantly, and the sectors $N_A = 4, S_z = \pm 2$ show no enhancement at all. The full-valence CAS and VMC-optimised wave functions balance competing effects that try to reduce charge fluctuations and enhance the anti-ferromagnetic correlations. The previously predicted anti-ferromagnetic correlations⁵ are qualitatively correct, but the entanglement spectrum provides a detailed quantitative picture. The eigenvalues of the largest charge fluctuations for the VMC-optimised wave function are severely reduced in comparison to the HF wave function, and unlike in the case of HF, it is open to interpretation as to whether this is a triple or quadruple bond. Regardless, the entanglement spectrum provides useful criteria for classifying groups of molecules, and as an example we consider the corresponding properties between the C_2 molecule and the Be_2 molecule. Both of these molecules have partial bonds in their HF wave functions as seen in Table 1, two inverted bonds as seen in Fig. 3, and anti-ferromagnetic behavior enhanced by

many-body effects as seen in the entanglement spectrum of Fig. 2 and Table 3. This suggests we can use the Be_2 molecule as a model for C_2 and possibly other more complicated systems in which we want to study the behavior of partial bonds.

To summarise, we have developed a new way to analyse covalent bonding in molecular systems. For HF wave functions, this reduces to a theory of electron fluctuations, but with a framework that allows for more complicated situations than MO theory, such as the inclusion of partial bonds. This analysis will be important to understand the differences between mean field theory simulations and many body simulations, especially for molecules that were previously difficult to characterise. We generalised our analysis for correlated wave functions, and identify a gapped structure of which the eigenvalues below the gap can be compared against model wave function entanglement spectra. We have provided detailed results of inverted bonds and anti-ferromagnetic correlations in the C_2 molecule, and our tools also allowed us to demonstrate that these bonds in C_2 observe the same physical properties as the bonds in Be_2 . All of the entanglement tools presented here are applicable to extended systems and more complicated bonding situations, which are not highly symmetric. We believe the full impact of these tools on *ab initio* systems will change how we approach electronic structure analysis in chemistry, physics, and materials science.

Methods

In the case of single-determinant wave functions, spatial density matrices can be calculated analytically^{20,25,26}. For wave functions beyond HF, quantum Monte Carlo methods are currently the only techniques for efficiently calculating the eigenvalues and eigenvectors of $\hat{\rho}_A$ and $\hat{\rho}_B$ for general continuum

wave functions in 2- and 3-dimensional systems²⁷. For methods to calculate the related Renyi entropies, there are several papers that describe techniques which have been applied to molecules, Fermi-Liquids, and spin models^{12, 14, 26–28}.

Quantum Monte Carlo simulations were done in our own code²⁴ which can run variational Monte Carlo, diffusion Monte Carlo and release-node quantum Monte Carlo. Our QMC code can import wave functions from the GAMESS package²⁹, which allowed us to simulate HF and full valence CAS wave functions. We separately implemented highly optimized VMC functions from a previous work^{23, 24}. HF and full-valence CASSCF simulations were run with the correlation-consistent polarized valence quadruple-zeta (cc-pVQZ) basis set³⁰. The entanglement natural orbitals for both the HF and CASSCF can be determined from the single-particle reduced density matrix (1-RDM)²⁷. We first obtain the full HF orbitals or natural orbitals by diagonalizing the 1-RDM. We divide our quantum system into two regions, A and B, and the natural orbitals are then projected onto a real space grid in region A, which are the matrix elements of the 1-RDM in a position basis. This matrix is then diagonalized, and the resulting set of singular values are read off as $\sqrt{\lambda}$ for each entanglement natural orbital. The matrix elements of the spatial density matrix can be calculated with the SWAP operator in variational quantum Monte Carlo. We use the entanglement natural orbitals to construct a basis in which to expand the spatial density matrix. The estimator for $\hat{\rho}_A$, explained in ref. 27, uses a replica trick in which a $6N$ -dimensional configuration space is used in order to calculate the matrix elements of $\hat{\rho}_A$.

1. Amico, L., Fazio, R., Osterloh, A. & Vedral, V. Entanglement in many-body systems. *Rev. Mod. Phys.* **80**, 517–576 (2008).
2. Shaik, S. *et al.* Quadruple bonding in C₂ and analogous eight-valence electron species. *Nat. Chem.* **4**, 195 (2012).
3. Shaik, S., Rzepa, H. S. & Hoffmann, R. One Molecule, Two Atoms, Three Views, Four Bonds? *Angew. Chem. Int. Ed.* **52**, 3020–3033 (2013).
4. Frenking, G. & Hermann, M. Critical Comments on “One Molecule, Two Atoms, Three Views, Four Bonds?”. *Angew. Chem. Int. Ed.* **52**, 5922–5925 (2013).
5. Xu, L. T. & Dunning, T. H. Insights into the perplexing nature of the bonding in c2 from generalized valence bond calculations. *J. Chem. Theory Comput.* **10**, 195–201 (2014).
6. Mayer, I. Bond order and valence indices: A personal account. *J. Comput. Chem.* **28**, 204–221 (2007).
7. Lennard-Jones, J. E. The electronic structure of some diatomic molecules. *Trans. Faraday Soc.* **25**, 668–686 (1929).
8. Kurashige, Y., Chan, G. K.-L. & Yanai, T. Entangled quantum electronic wavefunctions of the Mn₄CaO₅ cluster in photosystem II. *Nat Chem* **5**, 660–666 (2013).
9. Wiberg, K. Application of the Pople-Santry-Segal CNDO method to the cyclopropylcarbinyll and cyclobutyl cation and to bicyclobutane. *Tetrahedron* **24**, 1083–1096 (1968).
10. Bader, R. F. W. *Atoms in Molecules* (Clarendon Press, 1994).

11. Mottet, M., Tecmer, P., Boguslawski, K., Legeza, O. & Reiher, M. Quantum entanglement in carbon-carbon, carbon-phosphorus and silicon-silicon bonds. *Phys. Chem. Chem. Phys.* **16**, 8872–8880 (2014).
12. McMinis, J. & Tubman, N. M. Renyi entropy of the interacting Fermi liquid. *Phys. Rev. B* **87**, 081108 (2013).
13. Vidal, G., Latorre, J. I., Rico, E. & Kitaev, A. Entanglement in quantum critical phenomena. *Phys. Rev. Lett.* **90**, 227902 (2003).
14. Hastings, M. B., González, I., Kallin, A. B. & Melko, R. G. Measuring Renyi Entanglement Entropy in Quantum Monte Carlo Simulations. *Phys. Rev. Lett.* **104**, 157201 (2010).
15. Gioev, D. & Klich, I. Entanglement Entropy of Fermions in Any Dimension and the Widom Conjecture. *Phys. Rev. Lett.* **96**, 100503 (2006).
16. White, S. R. Density matrix formulation for quantum renormalization groups. *Phys. Rev. Lett.* **69**, 2863–2866 (1992).
17. Schollwöck, U. The density-matrix renormalization group in the age of matrix product states. *Ann. Phys.* **326**, 96 – 192 (2011).
18. Ryu, S. & Takayanagi, T. Aspects of holographic entanglement entropy. *Journal of High Energy Physics* **2006**, 045 (2006).
19. Jiang, H.-C., Wang, Z. & Balents, L. Identifying topological order by entanglement entropy. *Nat. Phys.* **8**, 902–905 (2012).

20. Peschel, I. Special Review: Entanglement in Solvable Many-Particle Models. *Braz. J. Phys.* **42**, 267–291 (2012). 1109.0159.
21. Giambiagi, M., Giambiagi, M. & Jorge, F. Bond index: relation to second-order density matrix and charge fluctuations. *Theor. Chim. Acta.* **68**, 337–341 (1985).
22. Li, H. & Haldane, F. D. M. Entanglement Spectrum as a Generalization of Entanglement Entropy: Identification of Topological Order in Non-Abelian Fractional Quantum Hall Effect States. *Phys. Rev. Lett.* **101**, 010504 (2008).
23. Filippi, C. & Umrigar, C. J. Multiconfiguration wave functions for quantum monte carlo calculations of first-row diatomic molecules. *J. Chem. Phys.* **105**, 213–226 (1996).
24. Tubman, N. M., DuBois, J. L., Hood, R. Q. & Alder, B. J. Prospects for release-node quantum monte carlo. *J. Chem. Phys.* **135**, 184109 (2011).
25. Cheong, S.-A. & Henley, C. L. Many-body density matrices for free fermions. *Phys. Rev. B* **69**, 075111 (2004).
26. Tubman, N. M. & McMinis, J. Renyi Entanglement Entropy of Molecules: Interaction Effects and Signatures of Bonding. *ArXiv e-prints* (2012). 1204.4731.
27. Tubman, N. M. & Yang, D. C. Calculating the entanglement spectrum in quantum Monte Carlo with application to ab initio hamiltonians. *Phys. Rev. B* **90**, 081116 (2014).
28. Swingle, B., McMinis, J. & Tubman, N. M. Oscillating terms in the Renyi entropy of Fermi gases and liquids. *Phys. Rev. B* **87**, 235112 (2013).

29. Schmidt, M. W. *et al.* General Atomic and Molecular Electronic Structure System. *J. Comput. Chem.* **14**, 1347 (1993).
30. Thom H. Dunning, J. Gaussian basis sets for use in correlated molecular calculations. i. The atoms boron through neon and hydrogen. *J. Chem. Phys.* **90**, 1007–1023 (1989).
31. Toulouse, J. & Umrigar, C. J. Full optimization of Jastrow–Slater wave functions with application to the first-row atoms and homonuclear diatomic molecules. *J. Chem. Phys.* **128**, 174101 (2008).

Acknowledgements We would like to thank T. Hughes, D. Ceperley, J. McMinis, H. Changlani, P. Abbamonte and L. Wagner for useful discussions. This work was supported by DARPA-OLE program and DOE DE-NA0001789. Computer time was provided by XSEDE, supported by the National Science Foundation Grant No. OCI-1053575, the Oak Ridge Leadership Computing Facility at the Oak Ridge National Laboratory, which is supported by the Office of Science of the U.S. Department of Energy under Contract No. DE-AC05-00OR22725.

Contributions N.T. designed the project and wrote the skeletal version of the QMC code. C.Y. built on the original code to calculate the entanglement spectra using multi-configurational wave functions. N.T. and C.Y. both contributed to the writing of the manuscript.

Competing financial interests The authors declare no competing financial interests.

Corresponding author Correspondence to: Norm Tubman

Molecule	Electrons involved per bond type		
	Localised (0,0,1,1)	Partially bonded ($\lambda, \lambda, 1-\lambda, 1-\lambda$)	Delocalised (1/2,1/2)
H ₂			
Li ₂			
Be ₂			
C ₂			
N ₂			
F ₂			

Table 1: Bonding in the first row elements described by the Hartree-Fock wave function. The localised and the partially bonded electrons exist in groups of four, while the fully delocalised electrons exist in pairs. The partially bonded quadruplets are labelled with their corresponding values of λ .

Method	Energy (hartrees)
HF	-75.405 766
VB ⁵	-75.594 679
Full-Valence CAS	-75.643 166
MRCI+Q ⁵	-75.803 136
VMC ^{23, 24}	-75.8282(4)
FN-DMC ^{23, 24}	-75.8901(7)
RN-DMC ²⁴	-75.8969(1)
FN-DMC(2008) ³¹	-75.9106(1)
Estimated exact ^{23, 24}	-75.9265

Table 2: Ground state energies of C₂ for various electronic structure methods. The wave functions used in this work are indicated as shaded cells. The high quality VMC optimized wave function is more than 200 mHa lower in energy than the wave function used in VB theory. The most accurate results given by fixed-node diffusion Monte Carlo (FN-DMC) and release-node diffusion Monte Carlo (RN-DMC) are techniques in which the entanglement spectrum estimators can be implemented in future work.

Method	Eigenvalues	
	$N_A = 4 \pm 1$	$N_A = 4$
	$S_z = \pm 1$	$S_z = \pm 2$
Hartree-Fock	0.07373	0.00900
Full-Valence CAS	0.06460	0.02440
VMC	0.08394	0.03896

Method	Eigenvalues			
	$N_A = 6 \pm 3$	$N_A = 6 \pm 2$	$N_A = 6 \pm 1$	$N_A = 6$
	$S_z = \pm 1$	$S_z = \pm 2$	$S_z = \pm 3$	$S_z = \pm 4$
Hartree-Fock	0.00593	0.00605	0.00596	0.00144
Full-Valence CAS	0.00109	0.00508	0.01613	0.01564
VMC	0.00148	0.00557	0.01382	0.00832

Table 3: The entanglement spectrum dominant eigenvalues for the anti-ferromagnetic sectors in C_2 and Be_2 with different wave function types. The errorbar on the eigenvalues for the full-valence CAS and VMC are estimated to be no larger than 3×10^{-4} . The particle number in region A and S_z are the labels for the different sectors. The other eigenvalues for each of these anti-ferromagnetic sectors are orders of magnitude smaller, and thus are not presented here. For the anti-ferromagnetic sectors that are charge-neutral sectors or close to charge neutral, there is a significant increase in the dominant eigenvalue when compared to HF wave functions. For the sectors with large charge fluctuations, the eigenvalues are lessened because of Coulomb repulsion.

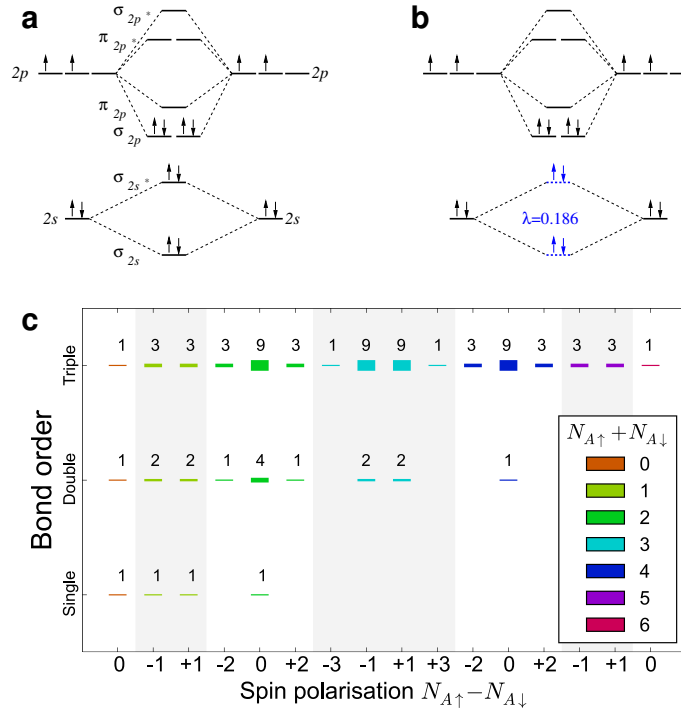


Figure 1 (a) Orbital hybridisation of the valence electrons in C₂ according to MO theory. The filling of three bonding and one anti-bonding orbital is a double bond in MO theory. (b) Modification of the hybridisation diagram with entanglement analysis. The λ values show that the pair of filled σ bonding and anti-bonding orbitals do not fully localise the associated electrons. A dashed line indicates that the two orbitals are paired, and the λ value is inserted between them to indicate the degree to which localisation occurs. (c) Entanglement spectra of the perfect bonding theory, in which all valence electrons are fully delocalised. Indicated above each bar is the number of eigenvalues in each block-diagonal sector of the spatial density matrix for these model wave functions. The vertical spread of each bar is proportional to the corresponding degeneracy. The sectors are labelled by the total number and spin polarisation of electrons (N, S_z) , where N is equal to the number of electrons. For real systems core orbitals and other localized orbitals might be present. These add extra electrons in region A and offset N by a constant. The magnitude of the eigenvalues are all equal with values, 0.25, 0.0625, and 0.0156 for a single bond, double bond, and triple bond respectively.

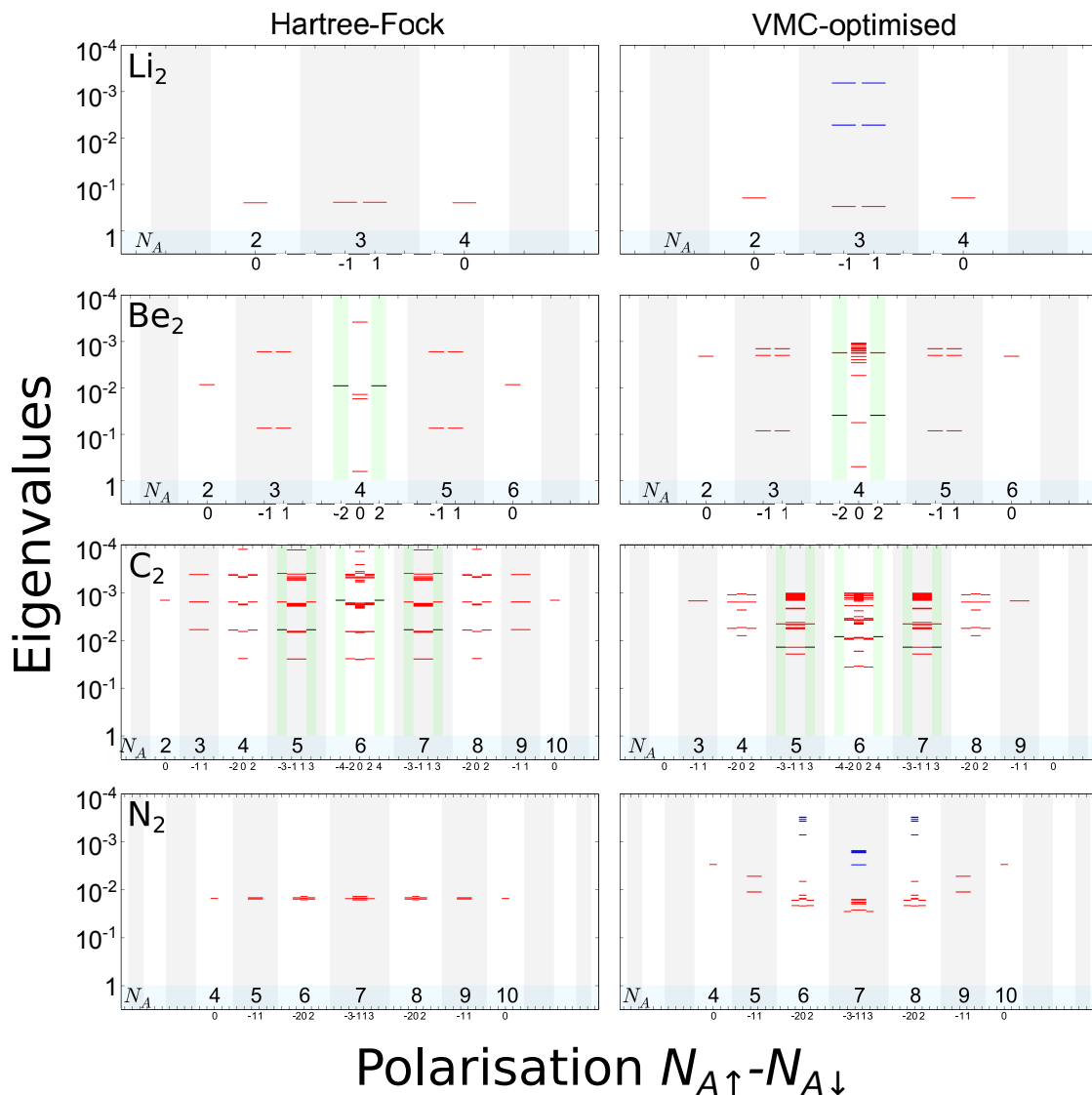


Figure 2 Entanglement spectra of Li_2 , Be_2 , C_2 , and N_2 . The left and right columns are based on the HF and VMC optimized wave functions, respectively. Errorbars on the eigenvalues are estimated to be no larger than 3×10^{-4} for the VMC optimized wave functions. The magnitudes of the eigenvalues are plotted on an inverted log scale. The larger an eigenvalue the more important it is. The HF wave functions for Li_2 and N_2 have entanglement spectra that correspond to perfect single and triple bonds, respectively. A gap opens up in each of their many-body entanglement spectra. The states above and below the gap are colored blue and red respectively. The Be_2 and C_2 molecules are more complicated due to the partial bonds. In comparing to the HF, the VMC optimized entanglement spectrum has an enhancement of anti-ferromagnetic fluctuations in both

of these molecules. The anti-ferromagnetic sectors are highlighted in green, and the most dominant eigenvalues in these sectors are colored black. The magnitude of these eigenvalues are given in Table 3.

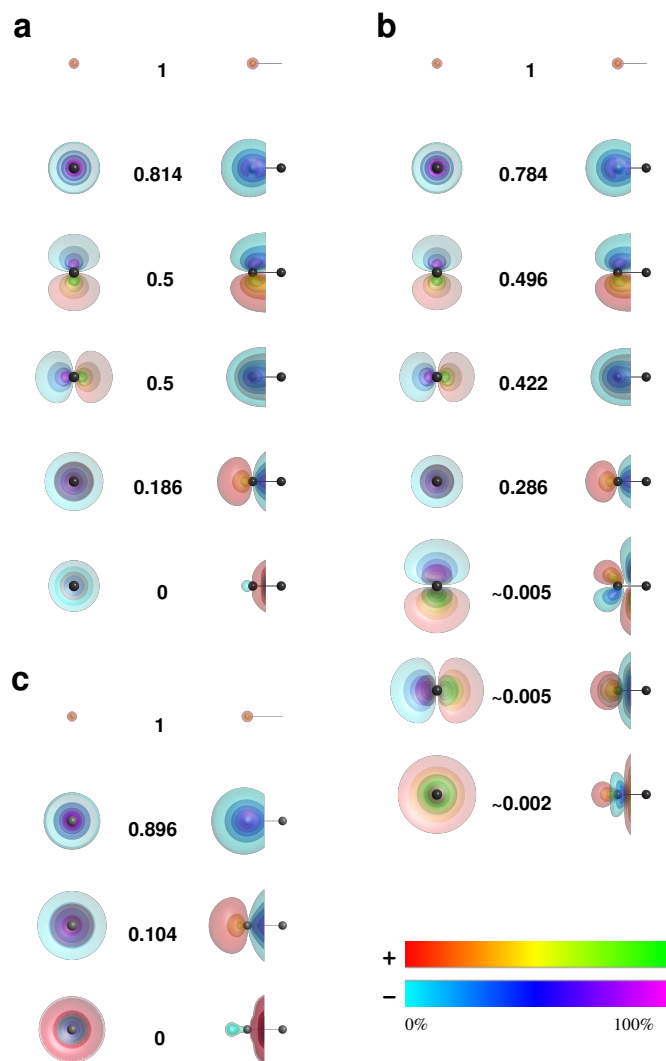


Figure 3 Isosurfaces of entanglement natural orbitals for (a) HF C_2 , (b) Full valence CAS C_2 , and (c) HF Be_2 . The numerical values are the λ values, as described in the text, for the HF wave functions, and they are the eigenvalues of the entanglement natural orbitals for the full valence CAS wave function. The plots show a view of the orbital along the bonding axis (left), and a side view of the bond (right). The isosurfaces were chosen by the amount of integrated density less than the isosurface value, which is indicated by the colour scale. There are actually 12 orbitals for the HF waveunfctions of C_2 and 8 orbitals for Be_2 , but only half are plotted as they are spin degenerate. The orbitals corresponding to $\lambda = 0.814$, 0.186 for HF C_2 , and $\lambda = 0.896$, 0.104 for HF Be_2 are inverted bonds. Corresponding orbitals of nearly identical character can be seen in the full valence CAS

C_2 orbitals with eigenvalues 0.784 and 0.286.